

---

# Latent Embeddings of Point Process Excitations

---

Myrl Marmarelis, Greg Ver Steeg, Aram Galstyan  
Information Sciences Institute  
University of Southern California  
myrlm@isi.edu, gregv@isi.edu, galstyan@isi.edu

## Abstract

When specific events seem to spur others in their wake, marked Hawkes processes enable us to reckon with their statistics. The underdetermined nature of these empirical mechanisms hinders estimation in the multivariate setting. Spatiotemporal applications alleviate this by allowing relationships to depend only on relative distances in real Euclidean space; we employ this framework as a vessel for embedding arbitrary event types in a new latent space. We demonstrate that learning the embedding alongside a point process model is resilient to ambiguities in the relationships among event types by performing synthetic experiments on short records as well as an investigation into options markets and pathogens.

## 1 Introduction & Motivation

The propagation of disease [1], news topics [2], crime patterns [3, 4], neuronal firings [5], and market trade-level activity [6, 7] naturally suit the form of diachronic point processes with an underlying causal-interaction network. Understanding their intrinsic dynamics is of paramount scientific and strategic value: a particular series of discrete options trades may inform an observer on the fluctuating dispositions of market agents; similarly, temporal news publication patterns may betray an ensuing shift in the public zeitgeist. The spread of a novel pathogen, notably the COVID-19 virus, through disjointed pockets of the globe hints to how it proliferates, and how that might be averted [8].

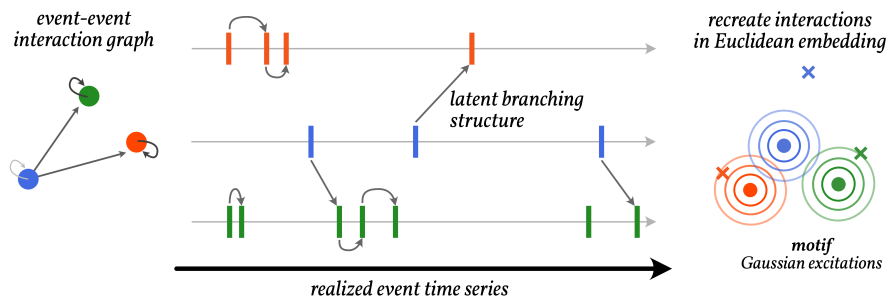


Figure 1: A stylized rendition. Instead of learning all possible interactions, we estimate a Euclidean embedding with fewer degrees of freedom and the additional benefit of interpretability.

Practically estimating the  $(n \times n)$  possible excitations between each dyad (pair) of event types is untenable without succinct and interpretable parametrizations. How can one possibly disentangle the contributions of hundreds of options trades within each minute, in a myriad of different strike prices and expiration dates, to the Poisson intensity of a particular type of trade? We must envision the right kind of bias for our model. Spatiotemporal domains [9, 3, 10] exploit physical constraints on interaction locality. In essence, the influence one event bears on another is governed solely by

their separation in space, invariant to absolute positioning. We show that it is feasible to conjure a *latent* spatial representation of the interacting event types by harnessing a spatiotemporal point process, and maximizing their joint likelihood. Much like word embeddings extracted from text corpora and graph embeddings from social networks, we tailor the latent space to capture the system under question: namely the precise interactions between events. Out-of-sample log likelihoods and a number of predictive metrics are improved with this structural imposition in applications that are both spatial and explicitly not spatial.

The conceived formulation for an excitatory—marked Hawkes [11]—point process permits tractable estimation with an expectation-maximization (EM) algorithm [12] that is commonly employed in identifying spatiotemporal Hawkes processes [10]. Most of the maximizations turn analytic when a latent branching structure is introduced that codifies potential causality. Its expectation is updated with respect to the current model at each EM iteration. See Figure 1 for a high-level schematic.

To our knowledge, we are the first to propose *a vector embedding scheme driven purely by an underlying point process*. We differ from recent event-sequence embedding techniques like [13] in our complete fusion of the event representation with the point process.

## 2 Method

**Formulation.** Consider a record of  $N$  event occurrences  $(k_i, t_i) \in \mathbb{H}$ ,  $i = 1, 2, \dots, N$ , with  $n$  marked types  $k_i \in \{1, 2, \dots, n\}$  at times  $t_i \in [0, T)$ . We have reason to believe that events with certain marks excite future events of either the same or another type. Multiple such interactions may be present, and we only want to identify those that are warranted by the observed record. A compact latent representation would induce a strong prior on the continuum of allowable interactions.

We start with preliminaries. The multivariate intensity function  $\lambda(k, t)$ , conditional on the events in  $[0, t)$ , dictates the instantaneous Poisson frequency. A particular interval  $[t, t + dt)$  would expect to witness  $\lambda(k, t)dt$  instances of event type  $k$ . We decompose this intensity [14] into self- and cross-excitations and a background rate intrinsic to the event type.

$$\lambda(k, t) = \sum_{i=1}^N h(k, k_i, t - t_i) + \mu(k). \quad (1)$$

One way to encourage skepticism about apparent interactions in the estimated response function  $h(k, l, \tau)$  is to constrain its structure. Suppose there exists a latent Euclidean geometry that adequately captures the interactions between event types. We infer distinct embeddings for receiving,  $x_k \in X \subset \mathbb{R}^m$ , versus influencing,  $y_l \in Y \subset \mathbb{R}^m$ , because otherwise we constrain our model to symmetrical bidirectional interactions—and that is not sufficiently expressive. Induced by a mapping on the marks,  $X$  and  $Y$  constitute the discrete embedding of a latent manifold wherein the influence some event type  $l$  exerts on  $k$  is characterized by  $\|y_l - x_k\|_2$ .

Each response is the result of a dyadic interaction between an event  $(k_i, t_i)$  in the past and the potential occurrence of event type  $k$  at the present time  $t$ . The chosen parametric family for the causal kernel bank entails Gaussian proximities in space and exponential clocks:

$$g_r(x, y) = (2\pi\beta_r^2)^{-\frac{1}{m}} \exp\left\{-\frac{\|x - y\|^2}{2\beta_r^2}\right\}, \quad (2) \quad f_r(\tau) = \delta_r e^{-\delta_r \tau}. \quad (3)$$

Eqs. 2 & 3 form the spatial and temporal basis of  $r = 1, 2, \dots, R$  kernels comprising the response function, tentatively produced here and fully expanded in Eq. 8. Later on we introduce the ingredients  $\xi(l)$  and  $\gamma_r$  for granularity in the magnitudes.

$$h(k, l, \tau) = \mathbb{1}[\tau > 0] \sum_{r=1}^R g_r(x_k, y_l) f_r(\tau).$$

A generalized Poisson process yields a clean log likelihood function, written as follows:

$$\log L = \sum_{i=1}^N \log \lambda(k_i, t_i) - \sum_{k=1}^n \int_0^T \lambda(k, t) dt. \quad (4)$$

However direct optimization on the basis of its gradient has proven unwieldy in anything other than deep general models. Even worse, its current form is not amenable to analysis.

Suppose we happened upon the expected *branching structure* [12] of the realized point process. In other words, we introduced latent variables  $[p_{ijr}] \in \mathbb{R}^{N \times N \times R}$  holding expectation estimates of  $P_{ijr} \in \{0, 1\}$ , indicating whether it was the event instance  $i$  that triggered instance  $j$ , and attributing responsibility to kernel basis  $r$ . Knowledge of the untenable true line of causation endows us with the so-called complete-data log likelihood termed  $\log L_c$  [10], an expectation of the joint log-probability density of the record and the latent variables  $[P_{ijr}]$  in terms of their probabilities  $[p_{ijr}]$ .

$$\log L_c = \sum_{j=1}^N \left( \sum_{i=1}^N \sum_{r=1}^R p_{ijr} \log h_r(k_j, k_i, t_j - t_i) + p_{bj} \log \mu(k_i) \right) - \sum_{k=1}^n \int_0^T \lambda(k, t) dt \quad (5)$$

By abuse of notation let  $h_r(\dots)$  denote the  $r$ th response kernel. Of special note in the above form is that what was previously a logarithm of summations (see Eq. 4 and 1) is replaced by a weighted sum of decoupled logarithms. The probability that the event instance was due to the background white Poisson process is  $p_{bj}$ ;  $\forall j, \sum_{i,r} p_{ijr} + p_{bj} = 1$ . Concretely, given a model  $\lambda(k, t)$ , the allegation of causality  $i \rightarrow j$  via  $r$  is the ratio of that particular contribution to the overall intensity:

$$p_{ijr} = \frac{h_r(k_j, k_i, t_j - t_i)}{\lambda(k_j, t_j)}. \quad (6)$$

The right-hand term in Eq. 5 simplifies vastly if one were to assume that  $\forall y_l \in Y \sum_{x_k \in X} g(x_k, y_l) = 1$ , and that  $\forall i \int_{t_i}^T f(t - t_i) dt \approx 1$ . The latter approximation is tenable; the former is not. Only through certain concessions may we gain confidence that the sum is roughly unit. First note that, by the Gaussian integral,  $\int_{\mathbb{R}^m} g(x, y) dx = 1$ . Veen & Schoenberg [9] arrived at the conclusion that this approximation holds arbitrarily well if the event occurrences in this putative space are distributed uniformly in  $\mathbb{R}^m$ . Our embedding scheme is usually not: events are clumped at discrete locations of their types, and we are left with a coerced normalization of Eq. 2;

$$\hat{g}_r(x, y) = \left[ \sum_{x' \in X} g_r(x', y) \right]^{-1} g_r(x, y). \quad (7)$$

We still rely on the “pure” form in Eq. 2 for the sake of closed-form optimization, as detailed below; nevertheless the surgery in Eq. 7 prevents drifting towards degeneracy. The final touch is the introduction of one more kernel parameter,  $\xi(l)$ , to account for this additional restriction. The full response kernel is therefore Eq. 8. We eliminated redundancies by constraining the *exertion coefficient*  $n^{-1} \sum_{l=1}^n \xi(l) = 1$  and scaling the *basis coefficients*  $\gamma_r$  appropriately.

$$h(k, l, \tau) = \mathbb{1}[\tau > 0] \sum_{r=1}^R \xi(l) \gamma_r \hat{g}_r(x_k, y_l) f_r(\tau). \quad (8)$$

## 2.1 Optimization

Furnished with the causality estimates in Eq. 6 (the “Expectation” step), we may perform projected gradient ascent by setting partial derivatives of the complete-data log-likelihood with respect to each kernel parameter to zero (the “Maximization” step). Eventually the causalities are aggregated in special ways to form coefficient estimates. Omitting the domains of summation over  $i$  and  $j$ ,  $i$  to imply  $\{1, 2, \dots, N\}$  and  $\{1, 2, \dots, N\} \times \{1, 2, \dots, N\}$  respectively, the solutions unfold as so:

$$\delta_r(\alpha_\delta, \beta_\delta) = \frac{\sum_{j,i} p_{ijr} + \alpha_\delta - 1}{\sum_{i,j} p_{ijr} (t_{k_j} - t_{k_i}) + \beta_\delta} \quad (9) \quad \gamma_r = \frac{\sum_{j,i} p_{ijr}}{\sum_i \xi(k_i)} \quad (11)$$

$$\beta_r^2 = \frac{\sum_{i,j} p_{ijr} \|x_{k_j} - y_{k_i}\|^2}{m \sum_{j,i} p_{ijr}} \quad (10) \quad \xi(l) = \frac{\sum_{r=1}^R \sum_{j,i} \mathbb{1}[k_i = l] p_{ijr}}{\sum_{r=1}^R \gamma_r \sum_i \mathbb{1}[k_i = l]}, \quad (12)$$

$$\mu(k) = T^{-1} \sum_j \mathbb{1}[k_j = k] p_{bj}. \quad (13)$$

Sometimes it is necessary to preserve focus on the acceptable time horizons for a particular domain, in bias against “degenerate” ones. A Gamma( $\alpha_\delta, \beta_\delta$ ) prior on the decay rate  $\delta_r$  admits the maximization a posteriori in Eq. 9, which trivially becomes uninformative at the assignment  $\delta_r(1, 0)$ . One is typically interested in the half-life ( $\log 2/\delta_r$ ), the prior of which is the reciprocal of the aforementioned gamma distribution and characterized by the aptly named inverse-gamma distribution with expectation  $\frac{\beta_\delta}{\alpha_\delta - 1}$ . Preserving the mean while increasing both parameters strengthens the prior.

The influence matrix  $\Phi = [\varphi(k, l)]$  is composed of the kernels with time integrated out, i.e.

$$\varphi(k, l) = \int_0^\infty h(k, l, \tau) d\tau = \sum_{r=1}^R \xi(l) \gamma_r g_r(x_k, y_l).$$

Persuant to the above maximization step, one may also optimize all of its degrees of freedom as

$$\varphi(k, l) = \frac{\sum_{j,i} \mathbb{1}[k_j = k, k_i = l] \sum_{r=1}^R p_{ijr}}{\sum_i \mathbb{1}[k_i = l]}. \quad (14)$$

## 2.2 Embedding in the Latent Space

**First Principles (FP).** We invoked the direct relation between the likelihood function and the embeddings. Our approach alternates between updating the reception embedding and the influence embedding, á la Gibbs sampling. Observe the partial gradient with respect to the vector  $y$ :

$$\begin{aligned} \frac{\partial \log L}{\partial y_l} = & \sum_{r=1}^R \left[ - \sum_{j,i} \mathbb{1}[k_i = l] p_{ijr} \left( \frac{y_l - x_{k_j}}{\beta_r^2} \right) \right. \\ & \left. + \xi(l) \gamma_r \sum_i \sum_{k=1}^n \mathbb{1}[k_i = l] (2\pi\beta_r^2)^{-m/2} \left( \frac{y_l - x_k}{\beta_r^2} \right) \exp \left\{ - \frac{\|y_l - x_k\|^2}{2\beta_r^2} \right\} \right] \quad (15) \end{aligned}$$

This behemoth is difficult to solve analytically. Recall, however, our prior simplifying assumption that  $\forall y, r \sum_{x \in X} g_r(x, y) = 1$ , also enforced a posteriori by means of Eq. 7. The latter portion of Eq. 15 contains the form  $\sum_x (x - y) g_r(x, y)$ , equivalent to taking a quantized “expectation” of a Gaussian variable subtracted by its own mean (see Eq. 2). Hence a viable approximation to a locally optimal  $y$  embedding point stems from neglecting the contribution of the entire second part of Eq. 15, allowing us to garner the following intuitive formula:

$$y_l = \frac{\sum_{r=1}^R \sum_{j,i} \mathbb{1}[k_i = l] p_{ijr} x_{k_j}}{\sum_{r=1}^R \sum_{j,i} \mathbb{1}[k_i = l] p_{ijr}}. \quad (16)$$

Evidently each influence point  $y \in Y$  is attracted to the reception points  $\{x \in X\}$  that appear to receive excitatory influence from it. Unfortunately there is no analogue approximation for the reception points themselves that could manifest by a similar sensible trick. We produce the derivation:

$$\frac{\partial \log L}{\partial x_k} = \sum_{r=1}^R \sum_i \left( \frac{x_k - y_{k_i}}{\beta_r^2} \right) \left[ - \sum_j \mathbb{1}[k_j = k] p_{ijr} + \xi(k_i) \gamma_r (2\pi\beta_r^2)^{-m/2} \exp \left\{ - \frac{\|x_k - y_{k_i}\|^2}{2\beta_r^2} \right\} \right] \quad (17)$$

and submit to regular gradient ascent with learning rate  $\varepsilon$ , and specifically an update rule along the average log likelihood for a consistent strategy across different record lengths:

$$x_k \leftarrow x_k + \varepsilon \cdot N^{-1} \frac{\partial \log L}{\partial x_k}. \quad (18)$$

To gain intuition on the selection of  $\varepsilon$ , we looked into *entropic impact* as a heuristic. The beautiful findings in [15] allowed us to reason about the following contribution of a change in an embedding point to the differential entropy of a doubly stochastic point process:

$$\frac{\partial^2 H(k, t)}{\partial t \partial x_k} = [\log \lambda(k, t) + 1] \sum_i \frac{\partial h(k, k_i, t - t_i)}{\partial x_k},$$

which admitted a simple rule of thumb to setting the learning rate proportional to  $\frac{h}{N}$ , with the constant pertaining to domain idiosyncrasies. Maintaining this ratio ameliorated convergence in §3.1.

**Diffusion Maps (DM).** Could we posit a diffusion process across event types? Random walk methods yield approximate manifold embeddings, proven helpful in deep representations [16, 17, 18]. Construed as graph affinities, the influences  $\Phi$  guide a Markovian random walk of which diffusion maps [19, 20, 21] may be approximated via spectral decomposition. We found that asymmetrical diffusion-maps embeddings (in the style of [22]) serve as an adequate initial condition but are not always conducive to stable learning in conjunction with our dynamic kernel basis. We term the model learned entirely this way as DM, and review briefly the technique’s application in Appendix A; the curious reader is encouraged to peruse the theory presented in Coifman’s seminal publications [21].

**Baseline (B).** Did the reduction in degrees of freedom lend its hand to a more generalizable model of the point process? In order to motivate the reason for having an embedding at all—besides the gains in interpretability—we pitted the techniques FP and DM against the following:

$$h(k, l, \tau) = \varphi(k, l) \mathbb{1}[\tau > 0] \sum_{r=1}^R f_r(\tau), \quad (19)$$

having estimated the matrix entries  $\varphi(\cdot, \cdot)$  directly as above in Eq. 14.

### 2.3 Initialization

We guessed adequate initial conditions for the EM procedure with a fixed empirical protocol. The surmised influence matrix came by summing up correlations between event types.

$$\hat{\varphi}(k, l) = \sum_{i,j} \mathbb{1}[k_j = k, k_i = l] \cdot \hat{\delta} e^{-\hat{\delta}(t_j - t_i)} \quad (20)$$

Notice that it remains unscaled.  $\hat{\delta}$  was computed as the naive reciprocal inter-arrival time between event types  $\hat{t} = n(N-1)^{-1} \sum_{i=1}^{N-1} (t_{i+1} - t_i)$ . We justify this construction on basis of Eq. 9, which forms a weighted average over said arrival times to garner an optimal estimate for  $\delta_r^{-1}$ . We feed the result of Eq. 20 into the diffusion-maps algorithm in order to obtain our initial embeddings  $(\hat{x}, \hat{y}) \in \hat{X} \times \hat{Y}$ .  $\forall r \hat{\beta}_r^2$  is initialized at the mean dyadic squared distance in the embedding;  $\hat{\delta}_r = (r \hat{t})^{-1}$ , in which variety is injected to nudge the kernels apart;  $\hat{\gamma}_r = R^{-1}$  and finally  $\forall x, \hat{\mu}(x) = T^{-1} n^{-1} N$ .

## 3 Results

### 3.1 Synthetic experiments

We intended to stress-test the learning algorithm under small record sizes and numerous event types; we thereby contrived a number of scenarios with known ground-truth parameters sampled randomly. The underlying models had a single kernel  $R = 1$  in the response function and conformed to the prescriptions FP, DM, and B from §2.2. Each sampled model was simulated with the thinning algorithm (see e.g. [23] and their supplementary material) in order to generate a time-series record of specified length  $N$ . Reception and influence points were realized uniformly from a unit square ( $m = 2$ ). Spatial bandwidths  $\beta^2$  were granted a gamma distribution with shape  $\alpha = 1/\sqrt{n}$  and unit scale. Decay rates  $\delta$  were standard log-normal as were backgrounds  $\mu(k)$ , though scaled by  $1/n$ .

Stability [14] was ensured by setting  $\gamma = 1/\sqrt{n}$ , constraining the Frobenius norm  $\|\Phi\|_F = 1$  that upper-bounds the  $L^2$ -induced norm, which itself upper-bounds the spectral radius of the influences  $\rho(\Phi)$ , the real criterion.

In line with Goodhart’s Law [24], different facets of the model apparatus were scrutinized. First, we sought to determine whether the baseline tends to reach high in-sample likelihoods yet abysmal out-of-sample likelihoods, including extreme outliers. Specifically, not only are statistics on each likelihood important but also the relationship between the two. We thought to convey it through a total least squares [25] slope and centroid, followed by its root mean-square error (RMSE) in the first four outcome columns of Table 1. The centroid gives empirical means for train and test log  $L$ , and the slope how much the test varies with the train. Did our models recover the chain of causation? We opened up the empirical  $[p_{i,jr}]$  estimates and computed their Hellinger distance [26] from those stipulated by the ground truth. For each “to be caused” event  $j$ , the quantities  $(i, r) \mapsto p_{i,jr}$  are framable as a discrete probability distribution. Its empirical construction makes it poorly suited numerically for the more widespread KL-divergence measure, unlike the Hellinger distance.

Settings	Outcomes							
	( $N$ )	( $n$ )	Ratio	Test	Train	Fit	Div.	Emb. Cor.
Model (see §2.2)	Events	Types						
FP ( $\epsilon = 0.75$ , Eq. 18)	300	15	1.09	-4.82	-4.36	0.68	0.14	*0.028
DM	300	15	1.47	-5.21	-4.52	0.61	0.12	***0.040
B	300	15	1.33	-5.34	-4.42	0.65	0.20	—
FP ( $\epsilon = 4.5$ )	300	90	2.85	-18.84	-8.05	1.29	0.39	0.002
DM	300	90	1.56	-10.01	-7.21	0.92	0.16	-0.005
B	300	90	5.13	-21.81	-6.83	1.17	0.77	—
FP ( $\epsilon = 0.25$ )	900	15	1.03	-5.79	-5.54	0.42	0.12	-0.012
DM	900	15	1.01	-3.94	-3.78	0.42	0.08	**0.044
B	900	15	1.10	-6.13	-5.71	0.54	0.14	—
FP ( $\epsilon = 0.5$ )	900	30	1.11	-4.45	-4.14	0.50	0.09	0.011
DM	900	30	1.09	-7.62	-7.04	0.63	0.11	*0.020
B	900	30	1.06	-6.87	-6.46	0.55	0.30	—
FP ( $\epsilon = 0.25$ )	1800	30	1.05	-5.12	-4.91	0.43	0.09	<b>-0.015</b>
DM	1800	30	1.11	-6.56	-6.20	0.51	0.08	<b>***0.053</b>
B	1800	30	1.07	-6.83	-6.53	0.42	0.22	—

Table 1: Agglomerate metrics collected in twenty simulated trials per synthetic experiment. A line fit by total least squares revealed an approximate test/train ratio. Outcome columns show, respectively, estimated test/train ratio (col. “ratio”), mean test and train log likelihoods (cols. “test” & “train”), RMSE of the fit line (col. “fit”), divergence from ground-truth causalities (col. “div.”), and mean correlation difference between the model and GloVe along with t-test significance markers (col. “emb. cor.”). \*\*\*:  $P \leq 0.01$ , \*\*:  $P \leq 0.05$ , \*:  $P \leq 0.1$ . Bold numerals indicate the sample rejected an Anderson-Darling test [27] for normality with significance  $\leq 0.05$ .

**Comparison to GloVe.** Our technique lives in a dual realm: that of vector embeddings for words and other sequential entities. We fed the ordered sequence of event-type occurrences into a typical GloVe scheme [28] with a forward-looking window of size three, three dimensions, and an asymmetric cooccurrence matrix in an attempt to recover a set of vectors that served as both influence and reception points.

The final column of Table 1 displays a systematic evaluation against GloVe’s embeddings with reference to the ground-truth geometry. Concretely, all pairwise distances in each setting (that of our learned model and the newfound GloVe embeddings) were correlated to those of the ground truth by Kendall’s rank-based nonparametric statistic [29]. The gap between GloVe’s estimated correlation and the model’s under scrutiny, each in  $[-1, 1]$  and where a positive difference means the model correlated more with the ground truth, was collected in each trial and means along with a t-test significance [30] were reported in the last column of Table 1. GloVe is nondeterministic, so we obtained the sample mean of ten embedding correlations per trial—a move that favors GloVe’s results. From the outcomes, it is evident that DM models pick up the spatial coordinates more consistently—probably due to the regularity imposed by their normalized spectral decomposition.

### 3.2 Real-world experiments

Model (see §2.2)	Best Train log $L$	Test log $L$	Half Life (days)	Best Epoch (0–999)
FP ( $\epsilon = 2$ in Eq. 18)	0.50	-1.18	8.02	179
DM	0.058	-1.80	19.27	202
B	0.87	-0.17	7.51	999
Geographic	0.33	-1.15	2.06	11
Salehi et al. [31]	—	-2.06	6.93	—

Table 2: Characterization of optimal models for the ebola dataset. Test and train log likelihoods are averages over  $N$ . Under  $R = 2$ , half lives were computed numerically.

**Ebola.** Disease contagion within any social apparatus tends to emerge as an excitatory point process. In 2019 a finely regularized variational approach to learning multivariate Hawkes processes from (a

little more than) a handful of data [31] was demonstrated on a dataset of symptom incidences during the ~2014-2015 ebola outbreak [32]. We gave the record precisely the same treatment they did, and obtained significantly higher commensurate likelihoods than their best case. We also trained a model with an embedding fixed to the geographic coordinates of the 54 West African districts present in the dataset, assessing the spatial nature of the process. See Table 2.

**Options market.** The intertwined market activity of options with underlying stocks TSLA, AAPL, and IBM during the arbitrary sequential trading days of September 15 & 18, 2017 lead to 24 distinct event types. Roughly 100,000 total trades per day were sampled on 120% and 80% fuzzy moneyness levels—as portrayed in Figure 2—at the expiration dates 01/18/2019 & 04/20/2018 for both puts and calls. The historical data was procured from AlgoSeek with the generosity of Prof. Roger G. Ghanem. The last 45 minutes of trading comprised each day’s test set. See Table 3: the auxiliary accuracy metric is derived from categorical cross-entropy of the predicted event type at the time of an actual occurrence, rendered by the expression

$$\exp\left\{\mathbb{E}_i \log \frac{\lambda(k_i, t_i)}{\sum_j \lambda(k_j, t_i)}\right\}.$$

We visualized three-dimensional embeddings via their two principal components in Figure 3.

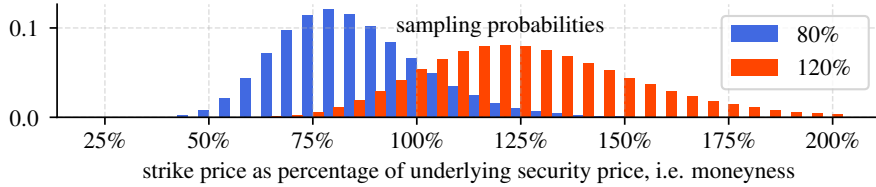


Figure 2: Trades at discrete strike prices were resampled according to quantized log-Gaussian profiles with reference to moneyness at any given point in time. Standard deviations, in logarithmic space, were half the separation between the two densities’ centers. They were kept “loose” for the sake of seamless translation even under abrupt fluctuations in the underlying stock price.

Dataset	Model	Best Train $\log L$	Test $\log L$	Half Life (min.)	Accuracy
Sep. 15	FP ( $\epsilon = 20$ )	3.05	<b>2.57</b>	$4.09 \times 10^{-4}$	0.119 vs. naive 0.099
	DM	2.85	2.34	$2.26 \times 10^{-4}$	0.103      0.099
	B	2.54	2.11	$1.15 \times 10^{-3}$	0.103      0.099
Sep. 18	FP ( $\epsilon = 1$ )	3.13	<b>2.72</b>	$5.88 \times 10^{-4}$	0.123 vs. naive 0.108
	DM	2.88	2.48	$2.32 \times 10^{-4}$	0.103      0.108
	B	2.75	2.43	$8.78 \times 10^{-4}$	0.117      0.108

Table 3: Market fits with associated half lives. In FP, the best in-sample  $\epsilon$  was picked out of a handful of candidates. Outcome of 200 epochs depicted. Accuracy is obtained from cross entropy.

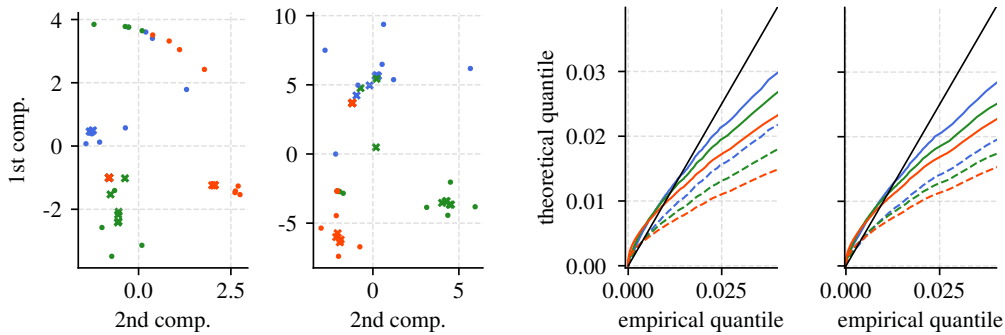


Figure 3: **Left: embeddings** on Sep. 15 and Sep. 18. Eight trade partitions per stock; TSLA is blue, AAPL green, and IBM orange. X’s receive; dots influence. Bandwidths are normalized to one. **Right: quantile plots**, Sep. 15 & 18, on inter-arrival times of all background (exogenous) market trades versus their supposed Exp. distributions with means that were empirical (solid) and model-derived (dashed), from the sum of all background rates. We depict the cases with no time prior.

## 4 Discussion

**Predictive ability.** Our class of models (even “B”) does not struggle with overfitting as much as deep and expressive ones might. Summarily we do not have a validation set, and display the epoch with the best training score in all our experiments. Most notable in Table 1 is how the DM formulation enjoys poorly determined systems, e.g. (300,90), but is typically outperformed on the basis of likelihoods by FP in better-posed situations like (900,30). The baseline suffers in recovering actual latent causalities (as depicted by their divergences from ground truth) in contrast to our models.

The ebola results in Table 2 depict superior results from all of our models to the state of the art. Whereas our EM “baseline” is best and the model with geographic ground truth performs marginally better than our FP, we count it as a positive that most of the information was retained. The strain afflicting the region during that period of time had an incubation period of about 8–12 days [33], suggesting preference for higher half lives. See our attempt at studying COVID-19 in Appendix B.

**Interpretation of the market embeddings.** Events belonging to each stock ticker tend to attract influencing points of the same color in Figure 3, with deviations hinting to their relative perceptions by the market. Efficient estimators are necessary in order to discern a lack of stationarity; in this case, transferring our Sep. 15 FP model onto the Sep. 18 test set yielded a log  $L$  improvement from 2.57 to 2.82, and vice versa gave a decrease from 2.72 to 2.45. Thus behavior largely persists.

The quantile plots put forth that both FP and DM outperformed the baseline in statistically filtering out the white (i.e. serially independent) background events according to their estimated probabilities  $p_{b,j}$ . A constant-intensity Poisson process would witness arrival times distributed exponentially [14].

**Disentangling time scales.** We unsuccessfully attempted to sway the estimators towards longer-term (on the order of seconds) behaviors by enlisting a prior on the exponential rate encouraging an expected half life of one minute. Parsing out minute-scale behaviors out of high-frequency trades is severely difficult—recall that most market makers dealing in options are automated. The Gamma prior inflicts a cost without influencing the half lives very much. It would be imperative to study higher-order interactions [34] if one were to investigate longer patterns through individual trades.

## 5 Related Work

The fundamental notion driving the doubly stochastic process, first attributed to Cox [35], manifests in a variety of ways including the particularly elegant Latent Point Process Allocation [36]. In fact, note the meteoric rise of work in Bayesian inference that now permeates serially dependent point processes. Zhang et al. [37] sample the branching structure  $p_{ij}$  (see Eq. 6) in order to carefully infer the underlying Gaussian process that constitutes the influence function. Gaussian processes, usually with latent inducing points, are also a prevailing assumption for the direct modulation of the intensity function [38, 36, 39, 40, 41]. Linderman and Adams [42] took an approach that estimated a matrix very similar to our  $[\varphi_{ijr}]$ , though relied on discretized binning and variational approximation—both of which we avoid. Salehi et al. [31] exploited a reparametrization trick akin to those in variational autoencoders in order to efficiently estimate the tensor of basis-function coefficients. Apostolopoulou et al. [43] augmented the excitatory model with a nonlinear term that enabled the full a posteriori inference of a model with inhibitions, sans variational approximation. A refreshing perspective on each pairwise interaction as its own process can be found in [44].

Recent progress has been made in factorizing the interaction space with a direct focus on scalability [45]. Additionally, there exist ventures in matching statistics of a Hawkes process with the observed record [14, 46, 47]. Notably Neural Hawkes [23] and a hodgepodge of other techniques centered around neural networks [48, 49, 50, 51, 52, 53, 2, 54, 55, 56] have been established through the years. Our baseline estimator resembles most closely the one described in the work of Zhou et al. [57], whereas the spatiotemporal aspect is inspired from the likes of Schoenberg et al. [9, 3, 10].

## 6 Conclusions

We demonstrated the viability of estimating embeddings for events optimized entirely on the point process dynamics. The proposed expectation-maximization algorithm extracts interpretable and parsimonious serial dependencies. Our framework paves the way for generalization, and extension to more elaborate models in the future.

## References

- [1] G. J. Gibson, G. Streftaris, and D. Thong, “Comparison and assessment of epidemic models,” *Statistical Science*, vol. 33, no. 1, pp. 19–33, 2018.
- [2] X. He, T. Rekatsinas, J. Foulds, L. Getoor, and Y. Liu, “Hawkestopic: A joint model for network inference and topic modeling from text-based cascades,” *International Conference on Machine Learning*, vol. 32, no. 37, pp. 871–880, 2015.
- [3] G. Mohler, “Marked point process hotspot maps for homicide and gun crime prediction in chicago,” *International Journal of Forecasting*, vol. 30, pp. 491–497, 2014.
- [4] G. O. Mohler, M. B. Short, P. J. Brantingham, F. P. Schoenberg, and G. E. Tita, “Self-exciting point process modeling of crime,” *Journal of the American Statistical Association*, vol. 106, no. 493, pp. 100–108, 2011.
- [5] J. W. Pillow, J. Shlens, L. Paninski, A. Sher, A. M. Litke, E. J. Chichilnisky, and E. P. Simoncelli, “Spatio-temporal correlations and visual signaling in a complete neuronal population,” *Nature*, vol. 454, pp. 995–999, 2008.
- [6] M. Morariu-Patrichi and M. S. Pakkanen, “State-dependent hawkes processes and their application to limit order book modeling,” *arXiv:1809.08060v2*, 2018.
- [7] A. Swishchuk and A. Huffman, “General compound hawkes processes in limit order books,” *Risks*, vol. 8, no. 28, 2020.
- [8] K. Drakopoulos, A. Ozdaglar, and J. N. Tsitsiklis, “When is a network epidemic hard to eliminate?,” *Mathematics of Operations Research*, vol. 42, no. 1, pp. 1–14, 2017.
- [9] A. Veen and F. P. Schoenberg, “Estimation of space-time branching process models in seismology using an em-type algorithm,” *Journal of the American Statistical Association*, vol. 103, no. 482, pp. 614–624, 2008.
- [10] B. Yuan, H. Li, A. L. Bertozzi, P. J. Brantingham, and M. A. Porter, “Multivariate spatiotemporal hawkes processes and network reconstruction,” *SIAM J. Math. Data Sci.*, vol. 1, no. 2, pp. 356–382, 2019.
- [11] A. G. Hawkes, “Spectra of some self-exciting and mutually exciting point processes,” *Biometrika*, vol. 58, no. 1, pp. 83–90, 1971.
- [12] P. F. Halpin and P. D. Boeck, “Modelling dyadic interaction with hawkes processes,” *Psychometrika*, vol. 78, pp. 793–814, October 2013.
- [13] M. Torricelli, M. Karsai, and L. Gauvin, “weg2vec: Event embedding for temporal networks,” *Scientific Reports*, vol. 10, no. 7164, 2020.
- [14] E. Bacry and J. F. Muzy, “First- and second-order statistics characterization of hawkes processes and non-parametric estimation,” *IEEE Transactions on Information Theory*, vol. 62, no. 4, pp. 2184–2202, 2016.
- [15] J. A. McFadden, “The entropy of a point process,” *Society for Industrial and Applied Mathematics*, vol. 13, no. 4, pp. 988–994, 1965.
- [16] D. Kalatzis, D. Eklund, G. Arvanitidis, and S. Hauberg, “Variational autoencoders with riemannian brownian motion priors,” *arXiv:2002.05227*, 2020.
- [17] H. Li, O. Lindenbaum, X. Cheng, and A. Cloninger, “Diffusion variational autoencoders,” *arXiv:1905.12724*, 2019.
- [18] L. A. P. Rey, V. Menkovski, and J. W. Portegies, “Diffusion variational autoencoders,” *arXiv:1901.08991*, 2019.

- [19] C. Soize and R. Ghanem, “Data-driven probability concentration and sampling on manifold,” *Journal of Computational Physics*, vol. 321, pp. 242–258, 2016.
- [20] W. Lian, R. Talmon, H. Zaveri, L. Carin, and R. Coifman, “Multivariate time-series analysis and diffusion maps,” *Signal Processing*, vol. 116, pp. 13–28, 2015.
- [21] R. R. Coifman and S. Lafon, “Diffusion maps,” *Applied and Computational Harmonic Analysis*, vol. 21, pp. 5–30, 2006.
- [22] K. Pham and G. Chen, “Large-scale spectral clustering using diffusion coordinates on landmark-based bipartite graphs,” *Workshop on Graph-Based Methods for Natural Language Processing*, vol. 12, pp. 28–37, 2018.
- [23] H. Mei and J. Eisner, “The neural hawkes process: A neurally self-modulating multivariate point process,” *31st Conference on Neural Information Processing Systems*, 2017.
- [24] C. Goodhart, *Inflation, Depression, and Economic Policy in the West*, ch. Problems of Monetary Management: The U.K. Experience, pp. 111–146. Rowman & Littlefield, 1981.
- [25] P. de Groen, “An introduction to total least squares,” *arXiv:math/9805076v1*, 1998.
- [26] T. Campbell and X. Li, “Universal boosting variational inference,” *33rd Conference on Neural Information Processing Systems*, 2019.
- [27] N. M. Razali and Y. B. Wah, “Power comparisons of shapiro-wilk, kolmogorov-smirnov, lilliefors and anderson-darling tests,” *Journal of Statistical Modeling and Analytics*, vol. 2, no. 1, pp. 21–33, 2011.
- [28] J. Pennington, R. Socher, and C. D. Manning, “Glove: Global vectors for word representation,” *Conference on Empirical Methods in Natural Language Processing*, 2014.
- [29] R. Newson, “Parameters behind “nonparametric” statistics: Kendall’s tau, somers’ d and median differences,” *The State Journal*, vol. 2, no. 1, pp. 45–64, 2002.
- [30] Student, “The probable error of a mean,” *Biometrika*, vol. 6, no. 1, 1908.
- [31] F. Salehi, W. Trouleau, M. Grossglauser, and P. Thiran, “Learning hawkes processes from a handful of events,” *33rd Conference on Neural Information Processing Systems*, 2019.
- [32] T. Garske, A. Cori, A. Ariyaratnam, I. M. Blake, I. Dorigatti, T. Eckmanns, C. Fraser, W. Hinsley, T. Jombart, H. L. Mills, G. Nedjati-Gilani, E. Newton, P. Nouvellet, D. Perkins, S. Riley, D. Schumacher, A. Shah, M. D. V. Kerkhove, C. Dye, N. M. Ferguson, and C. A. Donnelly, “Heterogeneities in the case fatality ratio in the west african ebola outbreak 2013-2016,” *Philosophical Transactions of the Royal Society B: Biological Sciences*, vol. 372, no. 1721, 2017.
- [33] M. D. V. Kerkhove, A. I. Bento, H. L. Mills, N. M. Ferguson, and C. A. Donnelly, “A review of epidemiological parameters from ebola outbreaks to inform early public health decision-making,” *Scientific Data*, vol. 2, no. 150019, 2015.
- [34] V. Z. Marmarelis and T. W. Berger, “General methodology for nonlinear modeling of neural systems with poisson point-process inputs,” *Mathematical Biosciences*, vol. 196, pp. 1–13, 2005.
- [35] D. R. Cox, “Some statistical methods connected with series of events,” *Journal of the Royal Statistical Society B*, vol. 17, no. 2, pp. 129–164, 1955.
- [36] C. Lloyd, T. Gunter, M. Osborne, S. Roberts, and T. Nickson, “Latent point process allocation,” *International Conference on Artificial Intelligence and Statistics*, vol. 19, no. 51, pp. 389–397, 2016.
- [37] R. Zhang, C. Walder, M.-A. Rizoio, and L. Xie, “Efficient non-parametric bayesian hawkes processes,” *International Joint Conference on Artificial Intelligence*, vol. 28, 2019.

- [38] S. Liu and M. Hauskrecht, “Nonparametric regressive point processes based on conditional gaussian processes,” *33rd Conference on Neural Information Processing Systems*, 2019.
- [39] V. Aglietti, E. V. Bonilla, T. Damoulas, and S. Cripps, “Structured variational inference in continuous cox process models,” *33rd Conference on Neural Information Processing Systems*, 2019.
- [40] H. Ding, M. E. Khan, I. Sato, and M. Sugiyama, “Bayesian nonparametric poisson-process allocation for time-sequence modeling,” *arXiv:1705.07006*, 2018.
- [41] S. Flaxman, M. Chirico, P. Pereira, and C. Loeffler, “Scalable high-resolution forecasting of sparse spatiotemporal events with kernel methods,” *arXiv:1801.02858*, 2019.
- [42] S. W. Linderman and R. P. Adams, “Scalable bayesian inference for excitatory point process networks,” *arXiv:1507.03228*, 2015.
- [43] I. Apostolopoulou, S. Linderman, K. Miller, and A. Dubrawski, “Mutually regressive point processes,” *33rd Conference on Neural Information Processing Systems*, 2019.
- [44] Y.-S. Cho, A. Galstyan, P. J. Brantingham, and G. Tita, “Latent self-exciting point process model for spatial-temporal networks,” *Discrete and Continuous Dynamical Systems Series B*, vol. 19, no. 5, pp. 1335–1354, 2014.
- [45] M. Nickel and M. Le, “Learning multivariate hawkes processes at scale,” *arXiv:2002.12501*, 2020.
- [46] M. Achab, E. Bacry, S. Gaïffas, I. Mastromatteo, and J.-F. Muzy, “Uncovering causality from multivariate hawkes integrated cumulants,” *International Conference on Machine Learning*, vol. 34, 2017.
- [47] J. Etesami, N. Kiyavash, K. Zhang, and K. Singhal, “Learning network of multivariate hawkes processes: A time series approach,” in *Proceedings of the Thirty-Second Conference on Uncertainty in Artificial Intelligence*, 2016.
- [48] Y. Lu, X. Wang, C. Shi, P. S. Yu, and Y. Ye, “Temporal network embedding with micro- and macro-dynamics,” *Proceedings of the Conference of Information and Knowledge Management*, 2019.
- [49] G. Loaiza-Ganem, S. M. Perkins, K. E. Schroeder, M. M. Churchland, and J. P. Cunningham, “Deep random splines for point process intensity estimation of neural population data,” *33rd Conference on Neural Information Processing Systems*, 2019.
- [50] M. Okawa, T. Iwata, T. Kurashima, Y. Tanaka, H. Toda, and N. Ueda, “Deep mixture point processes: Spatio-temporal event prediction with rich contextual information,” *KDD*, 2019.
- [51] T. Omi, “Fully neural network based model for general temporal point processes,” *33rd Conference on Neural Information Processing Systems*, 2019.
- [52] A. Sharma, A. Ghosh, and M. Fiterau, “Generative sequential stochastic model for marked point processes,” *ICML Time Series Workshop*, 2019.
- [53] J. Shang and M. Sun, “Geometric hawkes processes with graph convolutional recurrent neural networks,” *Association for the Advancement of Artificial Intelligence*, 2019.
- [54] N. Du, H. Dai, R. Trivedi, U. Upadhyay, M. Gomez-Rodriguez, and L. Song, “Recurrent marked temporal point processes: Embedding event history to vector,” *KDD*, 2016.
- [55] J. Jia and A. R. Benson, “Neural jump stochastic differential equations,” *33rd Conference on Neural Information Processing Systems*, 2019.
- [56] N. Mehrasa, R. Deng, M. O. Ahmed, B. Chang, J. He, T. Durand, M. Brubaker, and G. Mori, “Point process flows,” *arXiv:1910.08281*, 2019.
- [57] K. Zhou, H. Zha, and L. Song, “Learning triggering kernels for multi-dimensional hawkes processes,” in *Proceedings of the Thirtieth International Conference on Machine Learning*, 2013.